Lecture 3:
The H-Mode

AP 4990y Seminar
Columbia University
Spring, 2011

References

- Wagner et al. "Regime of improved confinement and high beta in neutral-beam-heated divertor discharges of the ASDEX Tokamak." Phys Rev Lett (1982) vol. 49 (19) pp. 1408-1412
- Wagner et al. "Development of an edge transport barrier at the H-mode transition of ASDEX." Phys Rev Lett (1984)
- Keilhacker et al. "Confinement studies in L and H-type Asdex discharges." Plasma Physics and Contr. Fusion (1984) vol. 26 pp. 49
- Keilhacker, et al., "The ASDEX divertor tokamak." Nuclear fusion (1985) (9) pp. 1045
- Doyle et al. "Chapter 2: Plasma confinement and transport." Nucl Fusion (2007) vol. 47 pp. S18-S127

ASDEX

1. INTRODUCTION: OBJECTIVES AND DESIGN CONSIDERATIONS

ASDEX, with major radius R = 1.65 m, small plasma radius a = 0.40 m, toroidal magnetic field $B_T \leqslant 2.8$ T and plasma current $I_p \leqslant 500$ kA, is one of the large second-generation tokamak experiments that were constructed in the 70s [1]. It was conceived as a divertor tokamak with the objective to test the potential of this scheme for controlling the particle and energy fluxes to the walls and for reducing impurities to a tolerable level. This called for a design that made the divertor physics as clear as possible but also facilitated comparison with a conventional limiter tokamak. The choice was a double-null poloidal divertor preserving the axi-symmetry of the tokamak configuration (Axially Symmetric Divertor Experiment).,

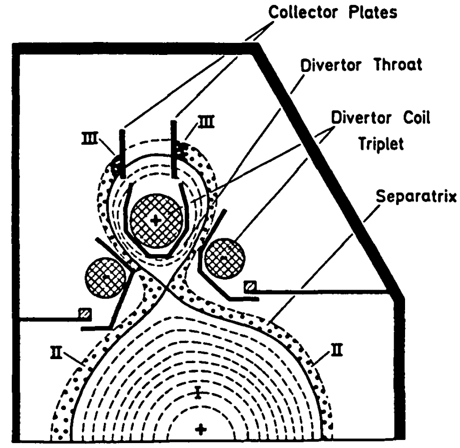

FIG.1. Cross-section of ASDEX (upper half).

ASDEX

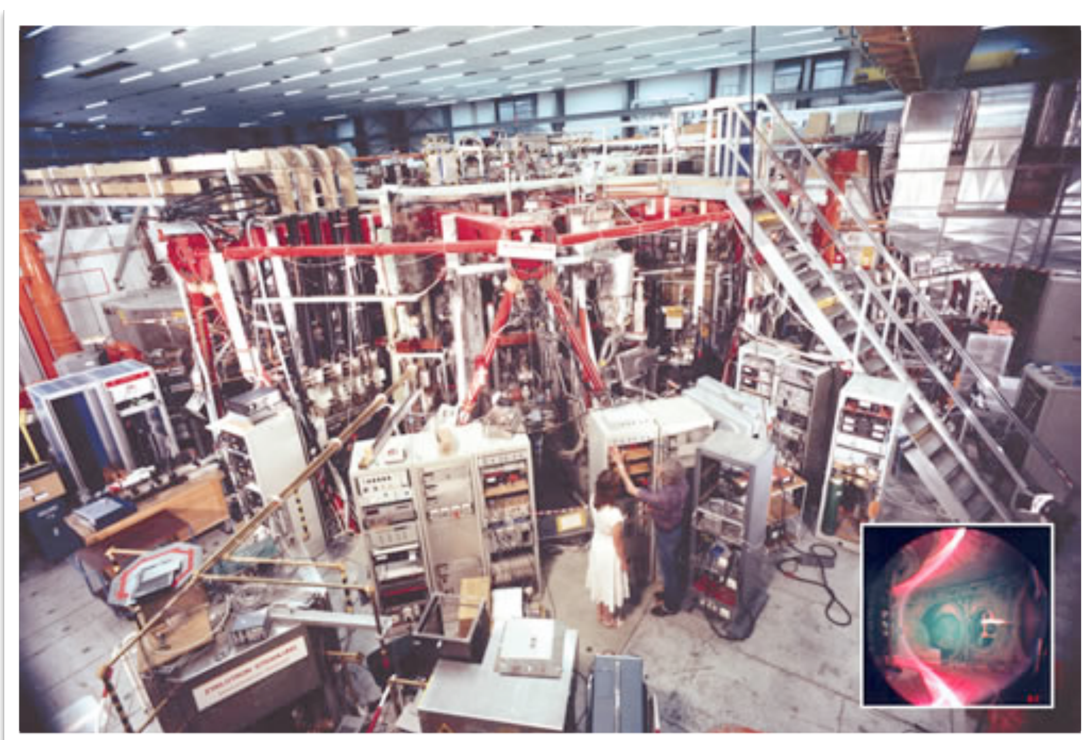

ASDEX

ITER-FEAT Outline Design Report
ITER Meeting, Tokyo, January 2000

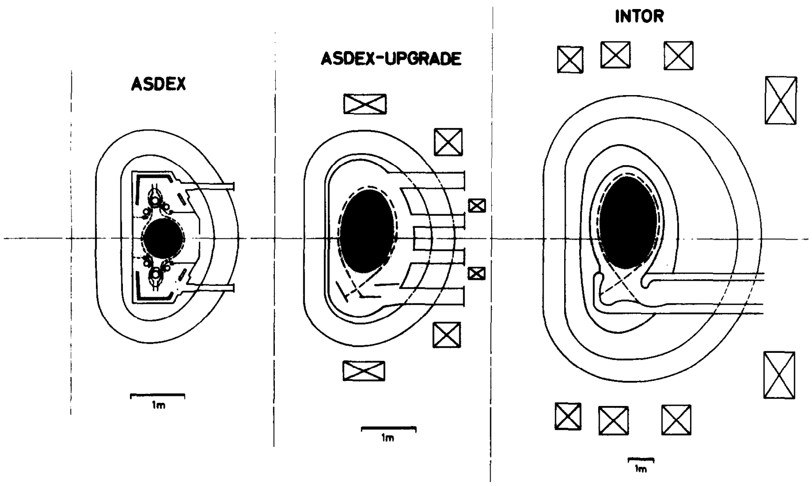

Fig. 1. ASDEX, ASDEX Upgrade and INTOR (~1/2 scale) in comparison.

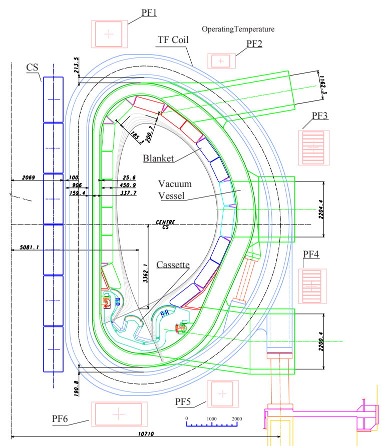

Figure 4.1 Cross-section of the ITER-FEAT tokamak

7

Regime of Improved Confinement and High Beta in Neutral-Beam-Heated Divertor Discharges of the ASDEX Tokamak

F. Wagner, G. Becker, K. Behringer, D. Campbell, A. Eberhagen, W. Engelhardt, G. Fussmann, O. Gehre, J. Gernhardt, G. v. Gierke, G. Haas, M. Huang,[a] F. Karger, M. Keilhacker, O. Klüber, M. Kornherr, K. Lackner, G. Lisitano, G. G. Lister, H. M. Mayer, D. Meisel, E. R. Müller, H. Murmann, H. Niedermeyer, W. Poschenrieder, H. Rapp, H. Röhr, F. Schneider, G. Siller, E. Speth, A. Stäbler, K. H. Steuer, G. Venus, O. Vollmer, and Z. Yü[a]
Max-Planck-Institut für Plasmaphysik, EURATOM-Association, D-8046 Garching, München, Germany
(Received 6 August 1982; revised manuscript received 1 October 1982)

A new operational regime has been observed in neutral-injection–heated ASDEX divertor discharges. This regime is characterized by high β_p values comparable to the aspect ratio A ($\beta_p \lesssim 0.65A$) and by confinement times close to those of Ohmic discharges. The high-β_p regime develops at an injection power $\gtrsim 1.9$ MW, a mean density $\bar{n}_e \gtrsim 3\times10^{13}$ cm^{-3}, and a $q(a)$ value $\gtrsim 2.6$. Beyond these limits or in discharges with material limiter, low β_p values and reduced particle and energy confinement times are obtained compared to the Ohmic heating phase.

PACS numbers: 52.55.Gb, 52.50.Gj

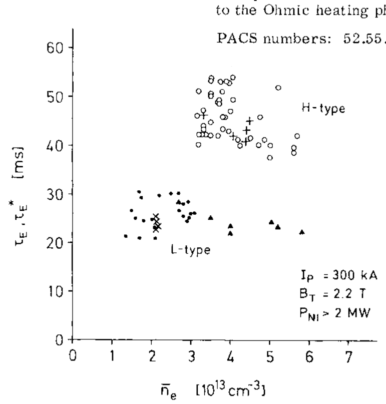

FIG. 2. Global energy confinement time vs average line density for toroidal limiter (triangles) and divertor discharges (other symbols). τ_E (plusses and crosses) is deduced from thermal profiles and τ_E^* (open circles, solid circles, and triangles) is determined from the diamagnetically measured $\beta_{p\perp}$.

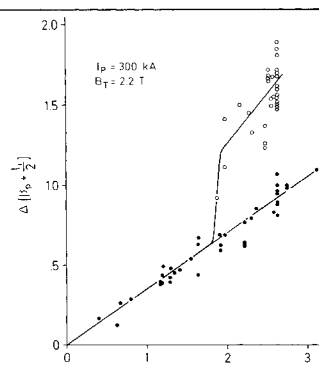

FIG. 3. Increase in $\beta_p + \frac{1}{2}l_i$ with respect to the Ohmic phase vs the power P_{NI} injected into the vessel in the L regime (solid symbols) and the H regime (open symbols).

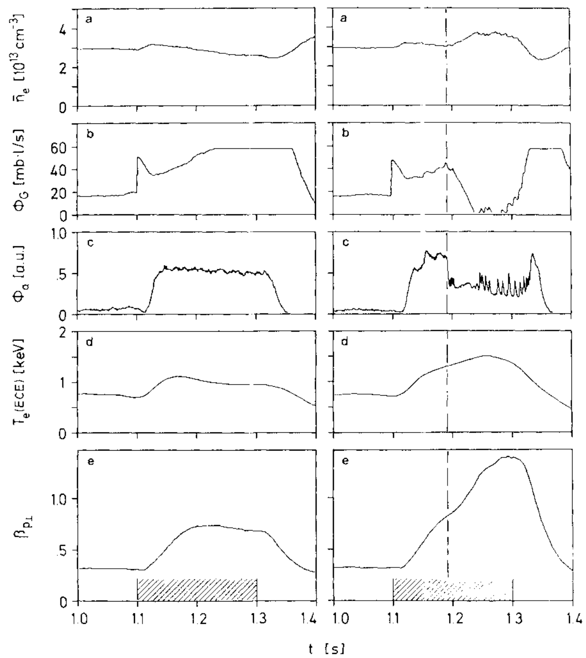

FIG. 1. Time dependence of various plasma parameters of L-type (left column) and H-type (right column) discharges: (a) line averaged density $\bar{n}_e$, (b) external gas flux φ_G, (c) atom flux φ_a ($E = 273$ eV) reflected from the divertor neutralizer plate, (d) central electron temperature, and (e) beta poloidal. The neutral injection phase is indicated by the hatched time interval. The dashed vertical line indicates the transition from the L to the H regime (see text).

VOLUME 53, NUMBER 15 PHYSICAL REVIEW LETTERS 8 OCTOBER 1984

Development of an Edge Transport Barrier at the H-Mode Transition of ASDEX

F. Wagner, G. Fussmann, T. Grave, M. Keilhacker, M. Kornherr, K. Lackner, K. McCormick, E. R. Müller, A. Stäbler, G. Becker, K. Bernhardi, U. Ditte, A. Eberhagen, O. Gehre, J. Gernhardt, G. v. Gierke, E. Glock, O. Gruber, G. Haas, M. Hesse, G. Janeschitz, F. Karger, S. Kissel, O. Klüber, G. Lisitano, H. M. Mayer, D. Meisel, V. Mertens, H. Murmann, W. Poschenrieder, H. Rapp, H. Röhr, F. Ryter, F. Schneider, G. Siller, P. Smeulders, F. Söldner, E. Speth, K.-H. Steuer, Z. Szymanski, and O. Vollmer

Max-Planck-Institut für Plasmaphysik–EURATOM Association, D-8046 Garching bei Müchen, West Germany

(Received 20 April 1984)

The thermal wave of a minor disruption can initiate the H phase of a neutral-beam–heated divertor tokamak discharge. Its propagation is used to probe the plasma edge conditions at the H transition. The results show the existence of a transport barrier which forms at the plasma edge and impedes the flow of particles and energy across the plasma surface, giving rise to improved confinement properties. Location and extension of the barrier coincide with the edge zone of increased shear specific to the divertor configuration.

PACS numbers: 52.55.Gb, 52.50.Gj

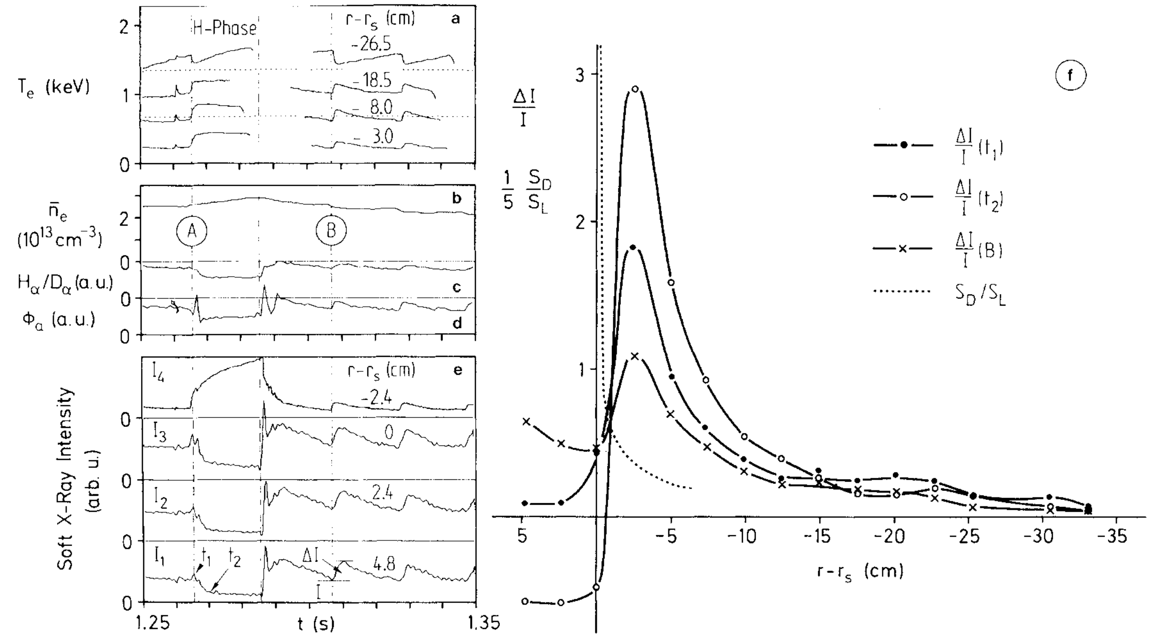

FIG. 1. Time evolution of (a) ECE electron temperature T_e (measured by electron cyclotron emission), (b) line-averaged density $\bar{n}_e$, (c) D_α radiation in the divertor, (d) backreflected flux ϕ_a from the neutralizer plate, and (e) four SX traces from the plasma edge. (f) Radial dependence of the normalized SX signals $\Delta I/I$ for three cases: a normal sawtooth (B), the sawtooth which triggers the H phase at t_1, and the one 3.5 ms later in the H phase at t_2. The dashed curve is the ratio of shear of the divertor to limiter configuration. (The ECE traces are interrupted by a chopper.)

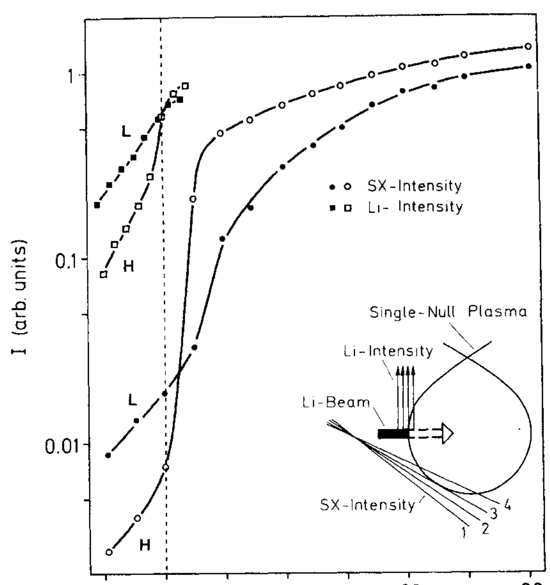

FIG. 2. Radial profiles of the SX (2-μm Be filter) and Li-beam intensities in the L phase prior to the H transition and shortly afterwards (SX, $\Delta t = 20$ ms; Li, $\Delta t = 55$ ms). $I_p = 375$ kA, $B_T = 2.2$ T, $\bar{n}_e = 3.3\times10^{13}$ cm^{-3}, $P_{NI} = 0.8$ MW. The inset depicts the observation geometry.

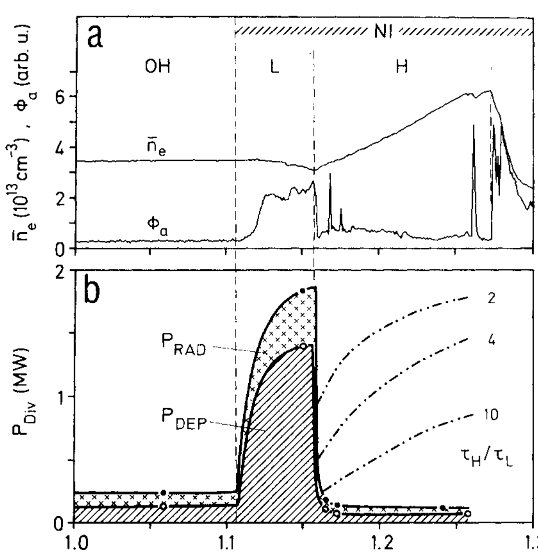

FIG. 3. (a) $\bar{n}_e$ and ϕ_a and (b) the total power flow P_{DIV} into the divertor chambers. The dashed-dotted curves show the variation of the normalized transport losses for energy confinement time changes at the H transition ($I_p = 315$ kA, $P_{NI} = 3.5$ MW).

The development of a perpendicular transport

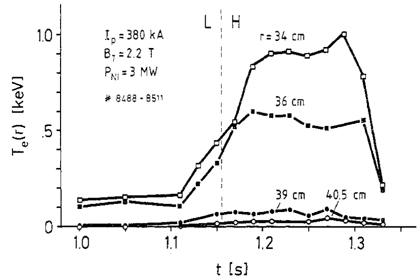

Fig. 2 Variation of electron temperature T_e at different radii at the plasma boundary during the NI phase (from 1.1 to 1.3 s).

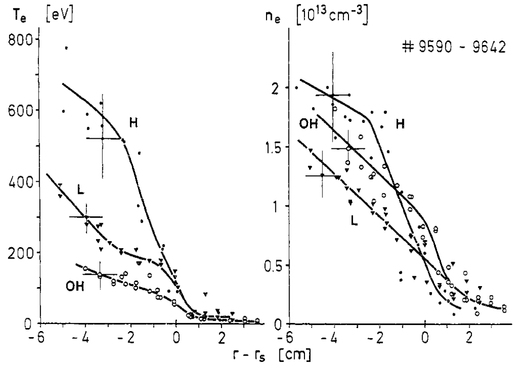

Fig. 3 Radial profiles of electron temperature T_e and density n_e at the plasma boundary for the 3 different confinement regimes OH, L and H. r_s is the separatrix radius. (The uncertainty in defining r_s is indicated by the horizontal error bars). I_p = 300 kA, $\bar{n}_e = 4 \times 10^{13}$ cm^{-3}, P_{NI} = 2.85 MW.

Plasma Physics and Controlled Fusion Vol.26 No.1A pp.49-63, 1984 0032-1028/84$3.00+ .00
Printed in Great Britain

CONFINEMENT STUDIES IN L AND H-TYPE ASDEX DISCHARGES

M. Keilhacker and G. Becker, K. Bernhardi, A. Eberhagen, M. ElShaer[1], G. Fußmann, O. Gehre, J. Gernhardt, G. v. Gierke, E. Glock, G. Haas, F.Karger, S. Kissel[2], O. Klüber, M. Kornherr, K. Lackner, G. Lisitano, G.G. Lister, J. Massig, H.-M. Mayer, K. McCormick, D. Meisel, E. Meservey[3], E.R. Müller, H. Murmann, H. Niedermeyer, W. Poschenrieder, H. Rapp, B. Richter, H. Röhr, F. Ryter[1], F. Schneider, G. Siller, P. Smeulders, F. Söldner, E. Speth, A. Stäbler, K. Steinmetz, K.-H. Steuer, Z. Szymanski[4], G. Venus, O. Vollmer, F. Wagner

Max-Planck-Institut für Plasmaphysik
EURATOM Association, D-8046 Garching

As indicated above, the critical parameter for the development of the H-regime seems to be the edge electron temperature (or the plasma resistivity). In order to surpass the required temperature threshold, the negative effects of cooling must be overcome by sufficient heating. This hypothesis has been checked by a number of experiments which are described in Ref. /6/. Here we only summarize the main results:

- The transition into the H-mode can be triggered by a sawtooth. In that case the heat pulse connected with the sawtooth increases the edge electron temperature above the critical value.
- If impurities are injected into the plasma, the resulting impurity radiation reduces the edge temperature and suppresses the H-mode (other cooling mechanisms, such as convection by enhanced recycling or heat conduction along a short connection length, e.g. to a limiter, have the same effect).
- A material limiter also reduces the edge temperature (owing to impurity radiation or recycling) and suppresses the H-mode.

The deleterious effect of a limiter is clearly seen from Fig. 4, which compares the variation of the edge electron temperature T_e (r = 31 cm) with the beam power P_{NI} in limiter discharges (poloidal carbon limiter) and divertor discharges (of the L and H-type). In the divertor configuration the edge temperature evolves without constraints, increasing linearly with P_{NI}. In limiter discharges, however, T_e (31 cm) is clamped to 150 - 200 eV, almost independently of the beam power. This shows why neutral-beam-heated limiter discharges are always of the low-confinement type.

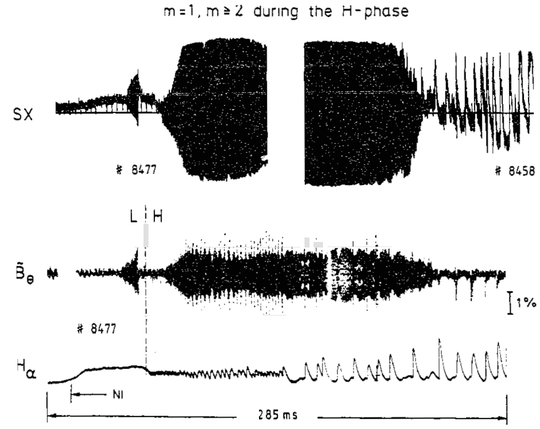

Fig. 10 Signals of a near centre soft X-ray detector (SX), an outside Mirnov loop ($\tilde{B}_\theta$) and an H_α/D_α detector (for reference) showing typical MHD behaviour (m = 1, m $\geq$ 2 modes; sawteeth) during the H-phase.

To summarize, we conclude that the H-transition does not depend on q_0 or q_a. The superior confinement properties of the H-phase rather allow broad electron temperature profiles with the consequence of broad current density profiles and $q_0 > 1$. Such profiles are very stable against all internal modes.

8. Edge Localized Modes

As already discussed in Sec. 2 and in the previous section, the H-phase is repeatedly interrupted by a new MHD phenomenon which severely limits the plasma temperatures and ß values attainable during this high-confinement mode. (The existence of this mode was already reported in ref. /1/.). Since the location of this MHD-phenomenon - as we will see - is at the plasma periphery, we call it the edge localized mode (ELM).

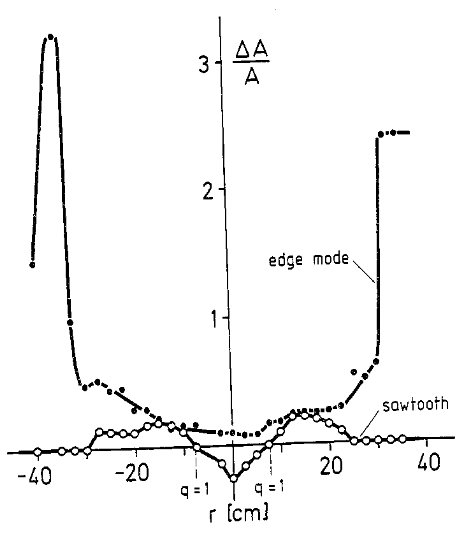

Fig. 12 Radial distributions of soft X-ray fluctuations connected with an edge localized mode and a sawtooth, respectively. The measurements indicate that the bursts are localized at the plasma edge.

As already mentioned in Sect. 2, the edge localized modes severely deteriorate the good particle and energy confinement of the H-phase, as can be seen on the density and $\beta_p{\perp}$ traces (c.f. Fig. 1). At each ELM the rise in density and $\beta_p{\perp}$ is terminated: the gain in particle and energy content between ELMs is lost at the ELM. This is similar to the effect of a sawtooth. While a sawtooth, however, is an internal mode which redistributes the energy in the plasma core thereby affecting global confinement only indirectly by shifting the gradients towards the plasma edge, an ELM is an external mode with a deteriorating effect on global confinement.

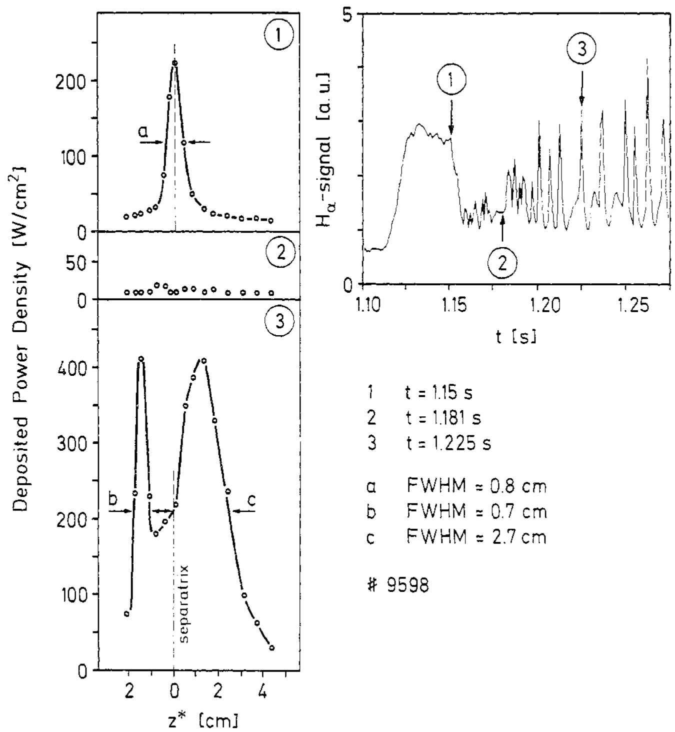

Fig. 13 Profiles of deposited power density onto an outer collector plate during different NI-phases: (1) L-phase, (2) quiet H-phase between bursts, and (3) at a burst. For comparison, the H_α/D_α-divertor radiation is shown. ΔZ is the distance from the intersection of separatrix and collector plate. $I_p = 320$ kA, $\bar{n}_e = 4 \times 10^{13}$ cm^{-3}, P_{NI} = 2.85 MW.

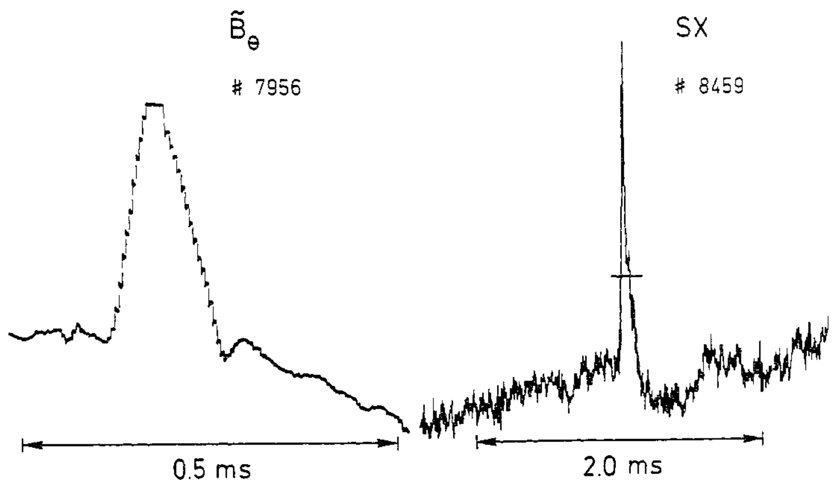

Fig. 14 Signals from a Mirnov loop ($\tilde{B}_\theta$) and a near centre soft X-ray detector (SX) showing the structure of an edge localized mode.

To summarize, we conclude that ELMs are MHD surface modes. Current density distributions corresponding to H-discharge temperature profiles are expected to be unstable to current driven (kink or tearing) modes with a resonance surface close to the outer edge of the strong gradient region. As this holds even for modes with relatively high m and n numbers (which are densely packed in q-space) these instabilities cannot easily be eliminated by a proper choice of the boundary q-value. The resonance surface will be in or close to the vacuum region, so that the growth rate of these modes might approach the kink time scale.

ExB Flow Shear Stabilization

REVIEW ARTICLES

Effects of $E\times B$ velocity shear and magnetic shear on turbulence and transport in magnetic confinement devices*

K. H. Burrell[†]
General Atomics, P.O. Box 85608, San Diego, California 92186-5608

(Received 13 November 1996; accepted 17 December 1996)

One of the scientific success stories of fusion research over the past decade is the development of the $E\times B$ shear stabilization model to explain the formation of transport barriers in magnetic confinement devices. This model was originally developed to explain the transport barrier formed at the plasma edge in tokamaks after the L (low) to H (high) transition. This concept has the universality needed to explain the edge transport barriers seen in limiter and divertor tokamaks, stellarators, and mirror machines. More recently, this model has been applied to explain the further confinement improvement from H (high) mode to VH (very high) mode seen in some tokamaks, where the edge transport barrier becomes wider. Most recently, this paradigm has been applied to the core transport barriers formed in plasmas with negative or low magnetic shear in the plasma core. These examples of confinement improvement are of considerable physical interest; it is not

I. INTRODUCTION

One of the scientific success stories of fusion research over the past decade is the development of the $E\times B$ velocity shear model to explain the formation of transport barriers in magnetic confinement devices. This model was originally developed to explain the transport barrier formed at the plasma edge in tokamaks after the L (low) to H (high) transition. As has been discussed previously,[1] this concept has the universality needed to explain the edge transport barriers seen in limiter and divertor tokamaks, stellarators, and mirror machines. More recently, this model has been applied to ex-

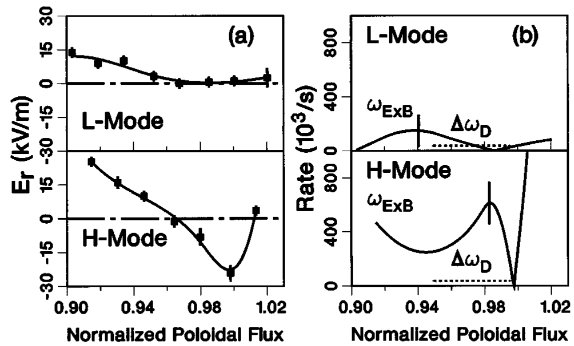

FIG. 5. Comparison of L-mode and H-mode edge profiles in DIII-D near the time of the L to H transition. The L-mode time is about 25 ms prior to the start of the dithering transition while the H-mode time is 50 ms later in the quiescent H-mode phase. In (a), the E_r profiles are shown; notice the characteristic E_r well at the plasma edge in H mode. In (b) the $E\times B$ shearing rate from Eq. (2) is compared to the intrinsic turbulence decorrelation rate. Because of the need to use several phase contrast chords to obtain the radial correlation length, the value is plotted as the average value over the region sampled. Plasma conditions are 1.5 MA plasma current, 2.2 T toroidal field, 8.6 MW injected deuterium neutral beam power, and 3.6×10^{19} m^{-3} line averaged density. Plasma is a double-null divertor operated in deuterium.

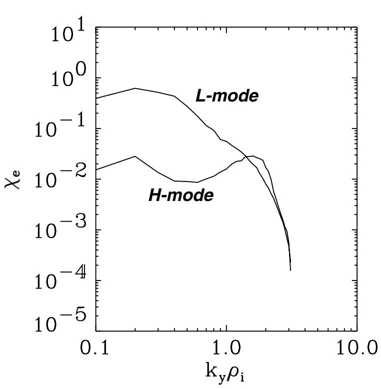

Figure 8. Gyro-kinetic simulations of tokamak edge turbulence without ('L-mode') and with ('H-mode') imposed $\vec{E}\times\vec{B}$ shear flows: the superposition principle for the electron heat diffusivity is violated, and ETG turbulence provides a floor in H-mode. Reprinted with permission from [140].

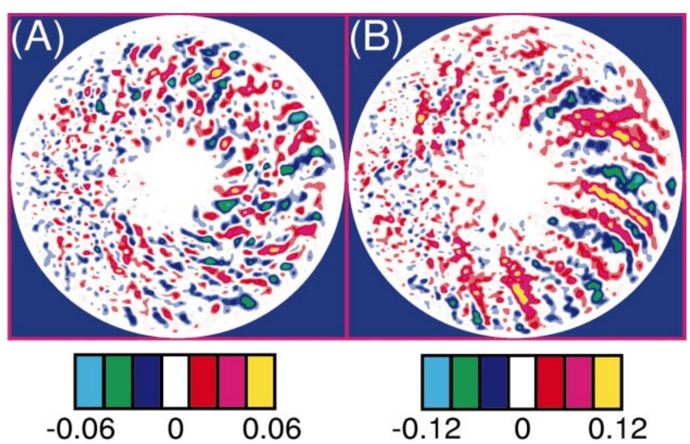

Fig. 2. Poloidal contour plots of fluctuation potential ($e\Phi/T_i$) in the steady state of nonlinear global simulation with **E** × **B** flows included (**A**) and with the flows suppressed (**B**). The dominant poloidal spectrum $k_\theta = 0$ mode is filtered out to highlight the differences in the turbulent eddy size.

MBER 1998 VOL 281 SCIENCE www.sciencemag.org

Turbulence level lower in H-mode at low-k (BES), and for $k_\perp \rho_s < 10$ (High-k scattering)

Drop in fluctuation power is ≈ 10db at lower frequencies.

Reduction in fluctuations not just at plasma edge, extend into plasma.

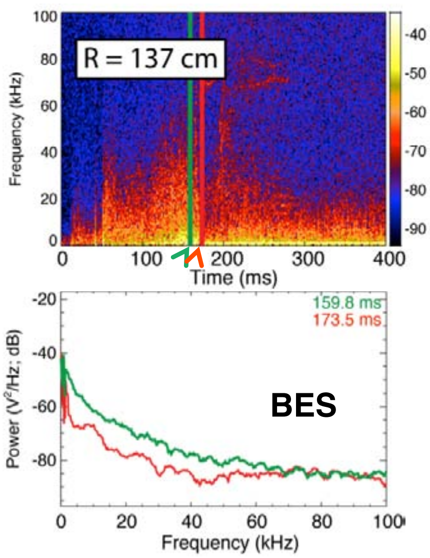

k spectra of normalized density fluctuations in beam-heated L and H-mode plasmas

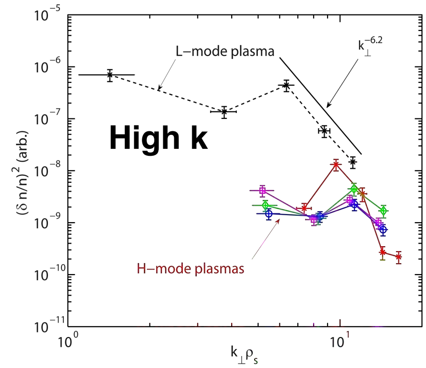

Spectral power for $k_\perp \rho_s$ >10 similar for L and H-mode.

Large differences, more than 2 orders of magnitude, in spectral power found at $k_\perp \rho_s$ <10 between L and H-mode.

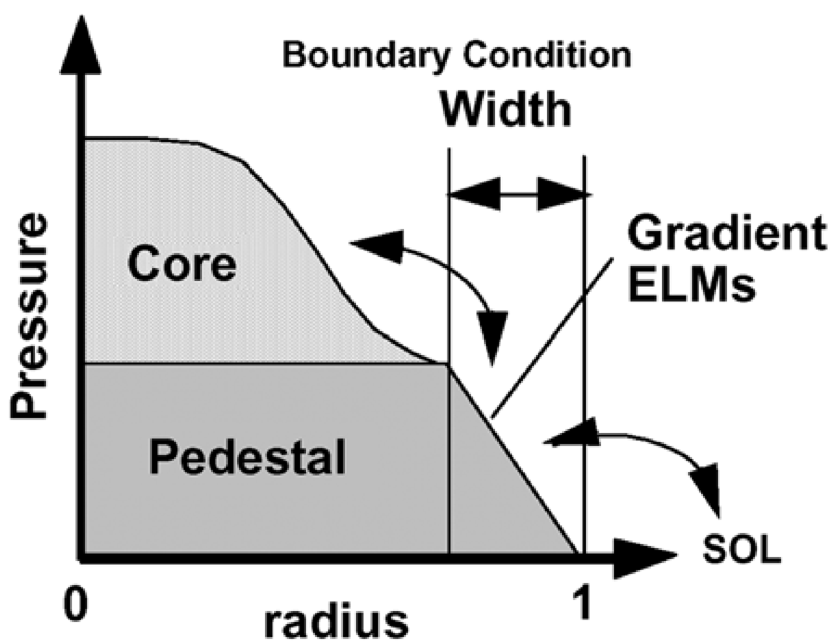

Figure 52. Schematic radial profile of plasma pressure.

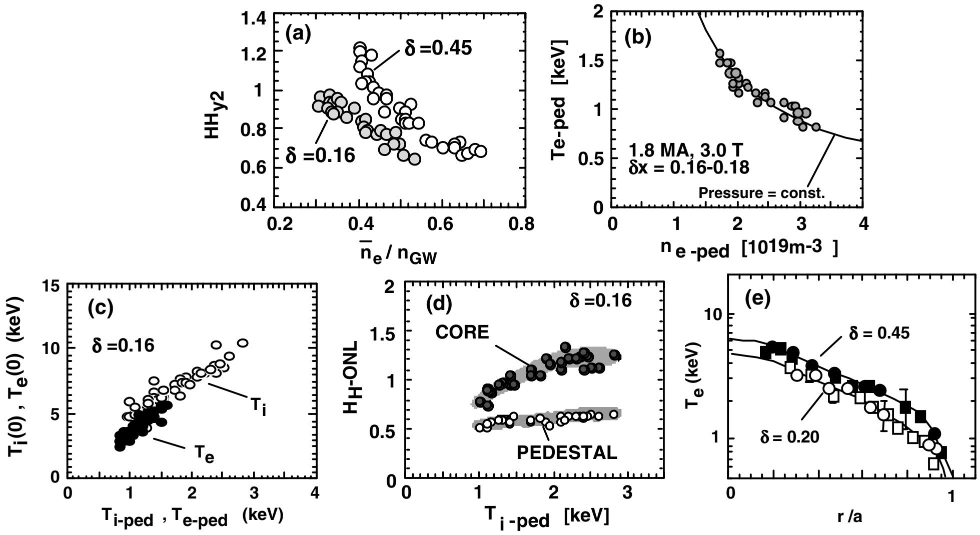

Figure 54. Type I ELMy H-mode in JT-60U [294]. (*a*) Density dependence of the HH_{y2}-factor for the Type I ELMy H-mode discharges (low-$\delta(=0.16)$, high-$\delta(=0.45)$). (*b*) Pedestal electron temperature as a function of pedestal electron density ($\delta = 0.16$). (*c*) Relationship between pedestal and central values of T_e and T_i. (*d*) Pedestal ion temperature dependence of confinement enhancement factors based on the offset non-linear scaling. (*e*) Comparison of the electron temperature profile for high and low δ cases with the same pedestal density.

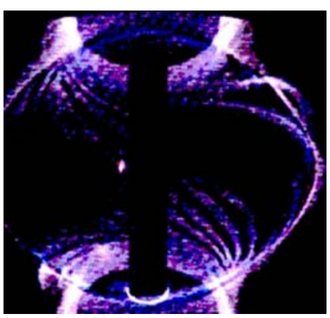

Figure 87. Filamentary structures observed in MAST during an ELM, consistent with the predictions of flux-tube eruptions from non-linear ballooning mode theory. Reprinted with permission from [555].

4.8.4. Implications for ITER. Clearly the understanding of ELM dynamics and associated phenomena have progressed significantly since the ITER Physics Basis. Nevertheless, a fully quantitative model for ELM size remains elusive. There

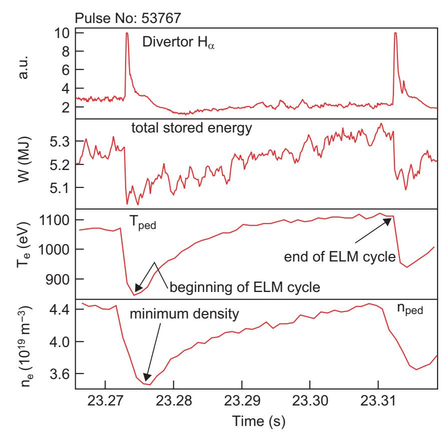

Figure 69. Example of a typical ELM cycle (Type I, JET). The time evolution of the D_α emission from the divertor, the plasma stored energy W, pedestal electron temperature T_e and density n_e are shown in boxes 1 to 4. The fast collapse of D_α, T_e and n_e at the ELM crash are highlighted by the arrow. Reprinted with permission from [497].

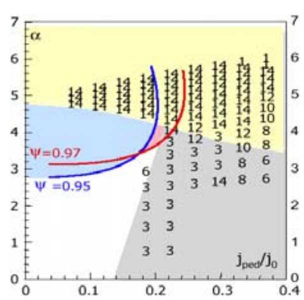

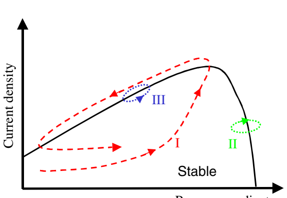

Figure 81. (*a*) Stability calculation for a JET discharge using the MISHKA code [670]. Shaded areas are unstable, numbers indicate the most unstable toroidal mode number calculated and the two curves indicate the $n = \infty$ ballooning stability boundary at two flux surfaces. α is the normalized pressure gradient and j_{ped}, j_0 are the current density in the pedestal region and centre, respectively. The grey area indicates the peeling or kink unstable region. The unshaded region is stable. (*b*) A sketch of the marginal stability curve (full curve), together with possible interpretations of large (I) and small (II and III) ELM cycles [666, 669].

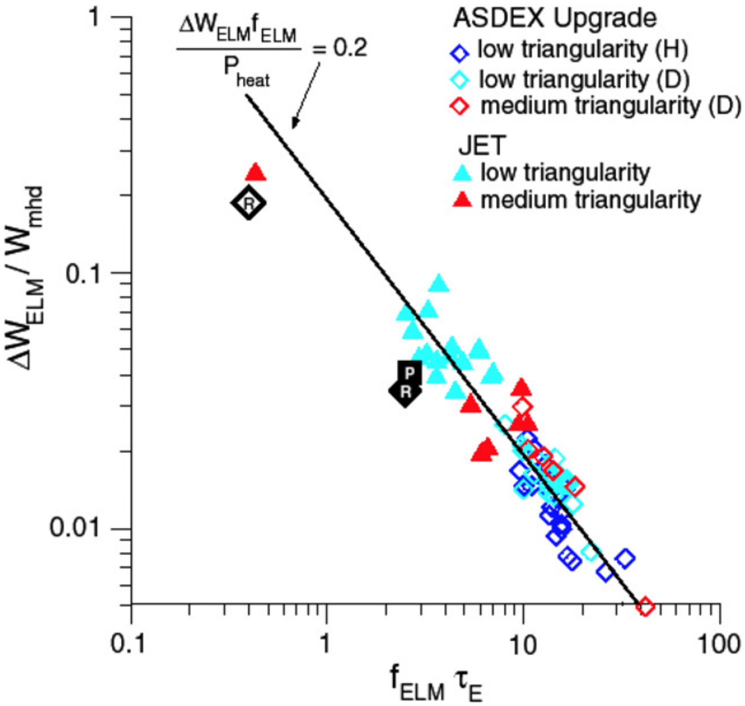

Figure 14. Comparison of ELM sizes obtained in this study for 19 Hz pellet triggered (P in filled black square) and 3 Hz (R in open black diamond) and 20 Hz (R in filled black diamond) intrinsic ELMs to values from a type-I ELM scaling for ASDEX Upgrade and JET [28].

Summary

The critical importance of the edge H-mode pedestal to overall plasma performance is increasingly recognized, and H-mode access is of course essential for ITER. Theory and modelling can now reproduce many aspects of the L–H transition but have not yet produced a reliable quantitative prediction for the power threshold. Consequently, global scaling techniques employing fits to experimental multi-machine data are still employed to project the L–H transition threshold power. Using an improved and expanded database the latest projection for ITER is a threshold power in the range ∼40–50 MW, within the capability of the ITER heating system (70 MW). Once in H-mode, global fusion performance is strongly influenced by the height of the edge temperature and density pedestals; with relatively stiff central

In an overall summary, it may be stated that both experimental and transport modelling/simulation indicate that ITER will meet its baseline design confinement requirements. Advanced operation on ITER with enhanced core confinement is becoming an increasingly realistic and attractive prospect, but a major experimental emphasis is required to demonstrate that such an advanced operation is compatible with reactor operating conditions. Substantial advances have been made in improving the physics content and reliability of transport modelling and simulation codes, but a fully consistent and integrated (core and edge) predictive capability which can accurately describe all transport channels is still some way in the future.